Neutron Scattering with a Triple-Axis Spectrometer

Basic Techniques

Gen Shirane, Stephen M. Shapiro, and John M. Tranquada
Brookhaven National Laboratory

CAMBRIDGE
UNIVERSITY PRESS

PUBLISHED BY THE PRESS SYNDICATE OF THE UNIVERSITY OF CAMBRIDGE
The Pitt Building, Trumpington Street, Cambridge, United Kingdom

CAMBRIDGE UNIVERSITY PRESS
The Edinburgh Building, Cambridge, CB2 2RU, UK
40 West 20th Street, New York, NY 10011–4211, USA
477 Williamstown Road, Port Melbourne, VIC 3207, Australia
Ruiz de Alarcón 13, 28014 Madrid, Spain
Dock House, The Waterfront, Cape Town 8001, South Africa

http://www.cambridge.org

© Cambridge University Press 2002

This book is in copyright. Subject to statutory exception
and to the provisions of relevant collective licensing agreements,
no reproduction of any part may take place without
the written permission of Cambridge University Press.

First published 2002

Printed in the United Kingdom at the University Press, Cambridge

Typeface Times 10/13pt *System* LaTeX [UPH]

A catalogue record of this book is available from the British Library

Library of Congress Cataloguing in Publication data

Shirane, G.
Neutron scattering with a triple-axis spectrometer / Gen Shirane, Stephen M. Shapiro,
and John M. Tranquada.
p. cm.
ISBN 0 521 41126 2
1. Neutrons–Scattering. I. Shapiro, S. M. (Stephen M.), 1941–
II. Tranquada, John M., 1955– III. Title.
QC793.5.N4628 S47 2002
539.7'213–dc21 2001035050

ISBN 0 521 41126 2 hardback

Contents

1

Introduction

In this introductory chapter we discuss some of the properties of the neutron and how it interacts with matter. We compare steady-state reactors to pulsed spallation neutron sources. After a review of the scattering geometry of an experiment we discuss the various instruments used for inelastic scattering.

1.1 Properties of thermal neutrons

The neutron is an ideal probe with which to study condensed matter. It was first discovered in 1932, and four years later it was demonstrated that neutrons could be Bragg diffracted by solids (see Bacon, 1986).† The early experimenters struggled with the low flux from Ra–Be sources but, nevertheless, established the fundamentals of neutron diffraction. The future was assured by the construction of the first "atomic pile" by Fermi and his co-workers in 1942. Subsequent reactors produced more and more neutrons and the latest generation of high-flux reactors built in the 1960s and early 1970s produce a copious number of neutrons, making inelastic scattering studies practical. It is now widely accepted that neutron scattering is one of the most important and versatile techniques for probing condensed matter. This fact was recognized by the awarding of the Nobel Prize in Physics in 1994 to Profs. C. Shull of Massachusetts Institute of Technology (MIT) and B. Brockhouse of McMaster University (Canada) for their seminal contributions to the fields of elastic and inelastic neutron scattering. Arguably the most important instrument used in neutron spectroscopy is the triple-axis spectrometer (invented by Brockhouse, 1961) since it allows for a controlled measurement of the scattering function $S(\mathbf{Q}, \omega)$ at essentially any point in momentum ($\hbar\mathbf{Q}$) and energy ($\hbar\omega$) space. (Here $\hbar$ is Planck's constant divided

† References are located at the end of each chapter.

Table 1.1. *Properties of the neutron.*

Quantity	Value
Rest mass, m_n	1.675×10^{-24} g
Spin	$\frac{1}{2}$
Magnetic moment, μ_n	1.913 nuclear magnetons, μ_N
Charge	0

by 2π, ω is 2π times the frequency ν, and the wave vector $\mathbf{Q}$ will be defined further in §1.3.)

Several of the properties of the neutron are listed in Table 1.1. The mass of the neutron is nearly that of the proton, and this relatively large mass has several important consequences. From the production viewpoint, the energetic neutrons produced by fission or spallation of heavy nuclei can be slowed down, or moderated, by collisions with atoms of similar mass, such as hydrogen or deuterium. The resultant energy distribution of the moderated neutrons is Maxwellian, with the average velocity determined by the temperature of the moderating medium. Another consequence of the large neutron mass is that "thermal" neutrons (i.e., those neutrons coming from a moderator near room temperature) have energies in an appropriate range (1–100 meV) for studying a wide variety of dynamical phenomena in solids and liquids.

The zero net charge of the neutron means that it interacts very weakly with matter and penetrates deeply into a sample. It also easily transmits through sample enclosures used to control the environment. This is a very important experimental convenience that is unique to the neutron probe. Even more important is the fact that with zero charge there is no Coulomb barrier to overcome, so that the neutrons are oblivious to the electronic charge cloud and interact directly with the nuclei of atoms. The theory of the interaction between a neutron and the nucleus of an atom is still incomplete, but it is known to be very short range ($\sim 10^{-13}$ cm $= 1$ fm, see Appendix 1). Since this is much less than the wavelength of thermal neutrons, the interaction can be considered nearly point-like. Therefore, neutron–nucleus scattering contains only s-wave components, which implies that the scattering is isotropic and can be characterized by a single parameter, b, called the scattering length. The typical value of the scattering length for the elements is on the order 1×10^{-12} cm, comparable to the nuclear radius. (The scattering cross section for a single nucleus is equal to $4\pi b^2$.) The scattering length can be complex; however, the imaginary part only becomes

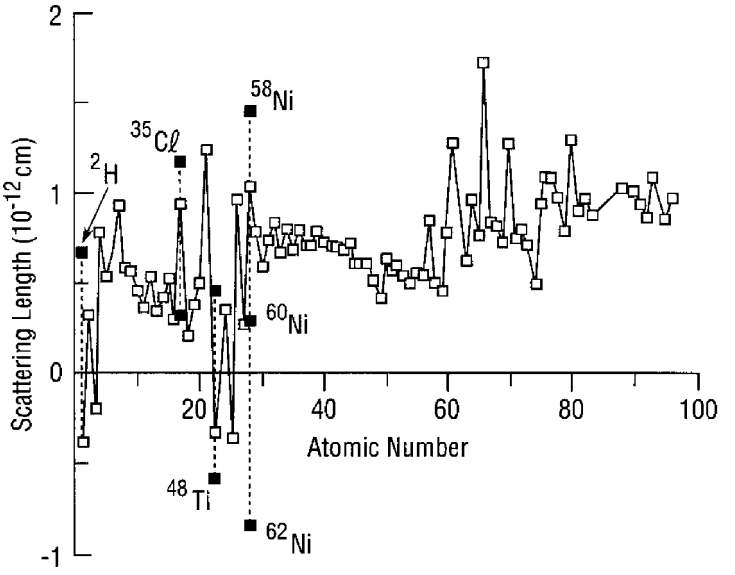

Fig. 1.1. Variation of coherent scattering length with atomic number (open squares). Variation of scattering length among isotopes of the same element is indicated for several cases by the filled squares. The coherent scattering length for an element corresponds to the average over all its isotopes, weighted by their abundance; the variations result in incoherent scattering, as discussed in Chap. 2 (from Price and Sköld, 1986).

significant near a nuclear absorption resonance. The real part is typically positive, but it can become negative at energies below a resonance; the sign of the scattering length is associated with the relative phase of the scattered neutron wave with respect to the incident wave. For most elements, the scattering length in the thermal energy regime is essentially independent of energy.

Figure 1.1 shows the variation of the scattering lengths for the different elements (Price and Sköld, 1986). (Appendix 1 tabulates these values.) One can see that most fall in the range between 0.2 and 1×10^{-12} cm. There is no systematic variation across the periodic table as there is for the case of X-ray or electron scattering. It is also seen that different isotopes of the same element can have different values of the scattering length, and can even be of different sign. The imaginary part of the scattering length represents absorption (principally radiative capture by the nuclei) and in most cases is small. Appendix 1 also lists the absorption cross sections for the elements. This quantity increases as the neutron energy approaches a nuclear resonance, so values must be quoted for a specific wavelength. Thus,

in contrast with electrons and X-rays, the scattering does not depend upon the number of electrons and its strength varies somewhat randomly among the elements, and among isotopes of the same element. Also, because of the weakness of the interaction, the scattering amplitude from a sample is equal to the sum of the scattering amplitudes of the individual atoms. This result simplifies the interpretation of measurements.

Although the neutron carries no net charge, its internal structure of quarks and gluons gives the neutron a magnetic moment. The neutron's magnetic moment, listed in Table 1.1, interacts with the unpaired electron spins in magnetic atoms with a strength comparable to that of the nuclear interaction. The neutron is, therefore, a powerful probe of magnetic properties of solids and has contributed enormously to our understanding of magnetism.

The effective magnetic scattering length, p, for a magnetic atom with a moment of n_{μ_B} Bohr magnetons is given by:

$$p = 0.27 \times 10^{-12} \times n_{\mu_B} \text{ cm.} \tag{1.1}$$

The constant is one-half of the classical radius of the electron multiplied by the gyromagnetic ratio of the neutrons. For $n_{\mu_B} \gtrsim 1$, it is apparent that p is comparable to the b values shown in Fig. 1.1 or, in other words, the scattered intensity associated with magnetic effects is comparable to the scattering from the nuclei.

With a spin angular momentum of $\pm\frac{1}{2}\hbar$ per neutron, neutron beams can be prepared which contain a single angular momentum state, either spin up ($+\frac{1}{2}\hbar$) or spin down ($-\frac{1}{2}\hbar$). These spin-polarized neutrons have unique applications in determining magnetic structures, separating magnetic from nuclear scattering, and isolating incoherent scattering from the total scattering.

1.2 Neutron sources

The neutrons used in a scattering experiment can be obtained from a nuclear reactor (Table 1.2), where the neutrons arise from the spontaneous fission of ^{235}U, or from a spallation source (see Table 1.3) where the neutrons are produced by bombarding a heavy target (e.g., U, W, Ta, Pb, or Hg) with high-energy protons (Windsor, 1981). In the former case, the neutrons are produced continuously in time, while in the latter, they typically come as pulses. The continuous flux of the current generation of high-flux reactors [High Flux Isotope Reactor (HFIR) at Oak Ridge National Laboratory, and High Flux Reactor (HFR) at the Institute Laue–Langevin (ILL), Grenoble] is $\sim 1 \times 10^{15}$ neutrons/cm^2 s. The first such reactor to be optimized for neutron-

beam research was the High Flux Beam Reactor (HFBR), see Fig. 1.2, at Brookhaven National Laboratory (BNL), which began operation in 1965. Although it is no longer operating, its design is typical of most high-flux reactors. In such a facility, the reactor, its auxiliary equipment, and the experimental facilities are contained in a sealed vessel of about 50 meters in diameter. This structure provides the final confinement against the escape of radioactive material into the environment. While the reactor is in operation the air pressure inside the building is kept slightly lower than atmospheric pressure outside to insure that any leakage is inward rather than outward. Access to the building is provided by a system of air locks.

Figure 1.2(b) shows a view of a segment of the experimental floor at the HFBR when it was operational. Neutrons from the reactor core were thermalized by a moderator of heavy water (D_2O); the thermalized neutrons reached the experimental floor through nine horizontal beam tubes. There were a total of 15 experimental facilities serving a wide variety of users. The newer neutron facilities, such as the HFR at ILL, Grenoble; Orphée at Laboratoire Léon Brillouin, Saclay; and the NIST Center for Neutron Research (NCNR) at the National Institute for Science and Technology near Washington, D.C., each have one or two "cold" sources. A cold source is a special moderator, typically utilizing liquid H_2 or CH_4 at cryogenic temperatures ($\sim$ 20 K), which shifts the peak of the Maxwellian distribution of neutrons to lower energy. The cold neutrons emerge in several beams; the separation between beams needed to allow for multiple instruments is achieved by transporting the neutrons over a long distance along slightly diverging paths into a "guide hall". For example, the HFR at ILL has, altogether, over 40 experimental facilities serving users in many disciplines.

At the pulsed sources (Table 1.3) neutrons are produced in bursts of roughly 10^{14} particles, with an initial pulse width on the order of 1 μs at a frequency of 10–50 Hz. The time-averaged, moderated flux at existing pulsed sources is considerably less than at steady-state, reactor-based sources; however (Table 1.4), the 2 MW Spallation Neutron Source (SNS) being built in Oak Ridge will be an order of magnitude more powerful than the most intense existing pulsed (non-fission) spallation source, ISIS. [An even more powerful source, the European Spallation Source (ESS) is under consideration in Europe.] The SNS time-averaged flux will be approximately one-third that of the most powerful research reactor, the HFR at ILL; however, the peak flux from a spallation source is much higher. Efficient use of the neutron-beam time structure compensates for the lower time-averaged flux (Windsor, 1981).

The energy spectra from the two types of sources are slightly different, as

Table 1.2. *Operating research reactors with flux* $\geq 10^{14}$ *neutrons*/(cm^2 s), *from the data base of the International Atomic Energy Agency* (http://www.iaea.org/worldatom/rrdb/).

Name	Institution	Location	Country	Year of Startup	Power (MW)
NBSR	National Institute of Standards and Technology (NIST)	Gaithersburg, MD	USA	1969	20
HFIR	Oak Ridge National Laboratory (ORNL)	Oak Ridge, TN	USA	1966	85
MURR	University of Missouri	Columbia, MO	USA	1966	10
HFBR	Brookhaven National Laboratory (BNL)	Upton, NY	USA	1965[a]	60
NRU	Chalk River Laboratories	Chalk River, Ontario	Canada	1957	120
HFR	Institute Laue Langevin (ILL)	Grenoble	France	1972[b]	58
Orphée	Commissariat a l'Energie Atomique (CEA)	Saclay	France	1980	14
BER-II	Hahn-Meitner Institute	Berlin	Germany	1973[b]	10
FRJ-2	Forschungszentrum Jülich	Jülich	Germany	1962	23
BRR	Budapest Neutron Center	Budapest	Hungary	1959[b]	10
WWR-M	Petersburg Nuclear Physics Institute (PNPI)	Gatchina	Russia	1960	18
R-2	Neutron Research Lab (NFL)	Studsvik	Sweden	1960	50
DR3	Risø National Laboratory	Risø	Denmark	1960[c]	10
MARIE	Institute of Atomic Energy	Swierk	Poland	1974	30
CFANR	Nuclear Research Institute	Rez	Czech Republic	1957	10
HFR	Interfaculty Reactor Institute (IRI)	Delft	Netherlands	1961	45
JRR3M	Japanese Atomic Energy Research Institute (JAERI)	Tokai	Japan	1990	20
HANARO	Korea Atomic Energy Research Institute (KAERI)	Taejon	Korea	1996	30
HIFAR	Australian Nuclear Science & Technology Organization	Lucas Heights	Australia	1958	10
MRR	National Nuclear Energy Agency	Tangerang	Indonesia	1987	30
HWRR-II	Institute of Atomic Energy	Beijing	China	1958	15
DHRUVA	Bhabha Atomic Research Centre	Trombay	India	1985	100

[a] Permanently shut down in 1999.
[b] Upgraded.
[c] Permanently shut down in 2000.

Table 1.3. *Operating spallation sources.*

Name	Institution	Location	Country	Year of Startup	Power (kW)
IPNS	Argonne National Laboratory	Argonne, IL	USA	1981	7
LANSCE	Los Alamos National Laboratory	Los Alamos, NM	USA	1985	180
ISIS	Rutherford–Appleton Laboratory	Oxfordshire	England	1985	160
IBR-2	Joint Institute of Neutron Research (JINR)	Dubna	Russia	1984	2000[a]
SINQ	Paul Scherrer Institute	Villigen	Switzerland	1996	1000[b]
KENS	High-Energy Laboratory (KEK)	Tsukuba	Japan	1980	3

[a] Fission.
[b] Continuous.

(a)

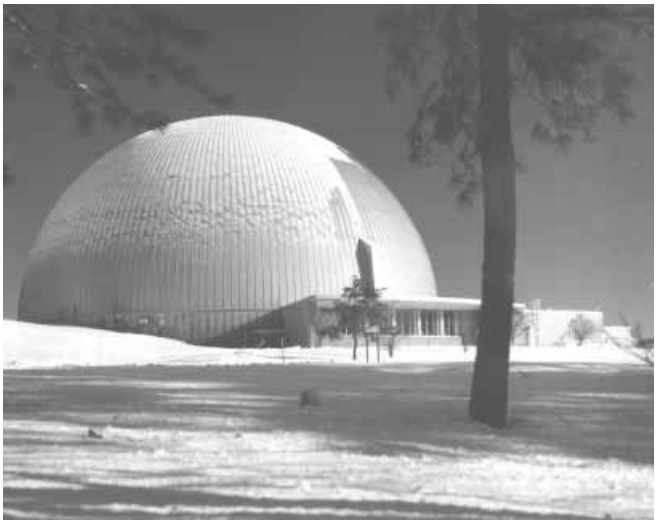

(b)

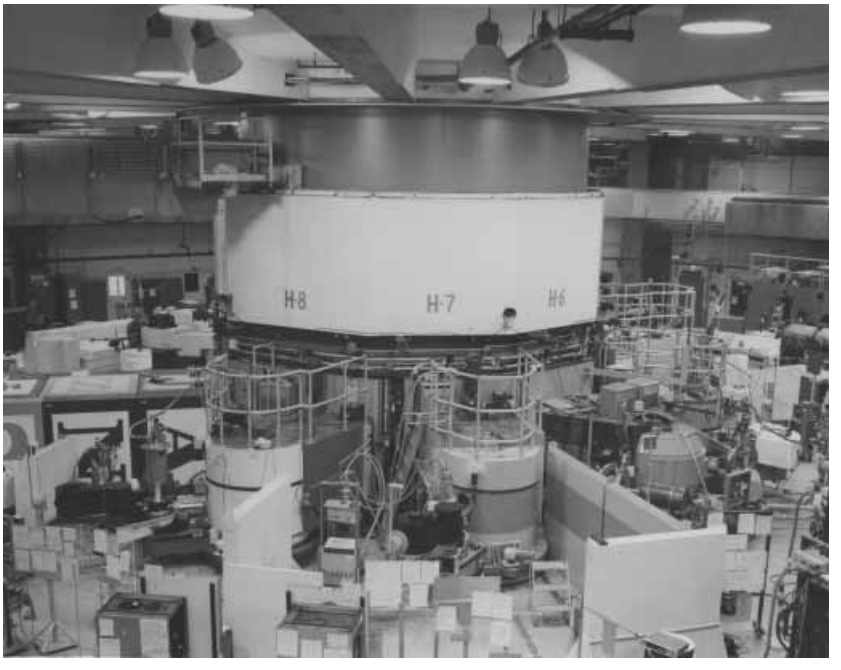

Fig. 1.2. (a) Photograph of domed building of Brookhaven's High Flux Beam Reactor and (b) a view of the experimental floor of HFBR during full operations.

Table 1.4. *New neutron sources.*

Name	Institution	Location	Country	Type	Power (MW)	Status
SNS	Oak Ridge National Laboratory	Oak Ridge, TN	USA	Pulsed	2	Under construction
FRM-II	Technical University of Munich	Garching	Germany	Reactor	20	Awaiting startup approval
AUSTRON			Austria	Pulsed	0.5	Under consideration
CNF	Chalk River Laboratories	Chalk River, ON	Canada	Reactor	40	Under consideration
ESS	European Science Foundation	Undecided	Europe	Pulsed	5	Under consideration
CARR	China Institute of Atomic Energy	Undecided	China	Reactor	60	Under consideration
RRR	ANSTO	Lucas Heights	Australia	Reactor	20	Under construction
JOINT PROJECT	JAERI	Tokai	Japan	Pulsed	2	Under construction
PIK	PNPI	Gatchina	Russia	Reactor	100	Awaiting completion

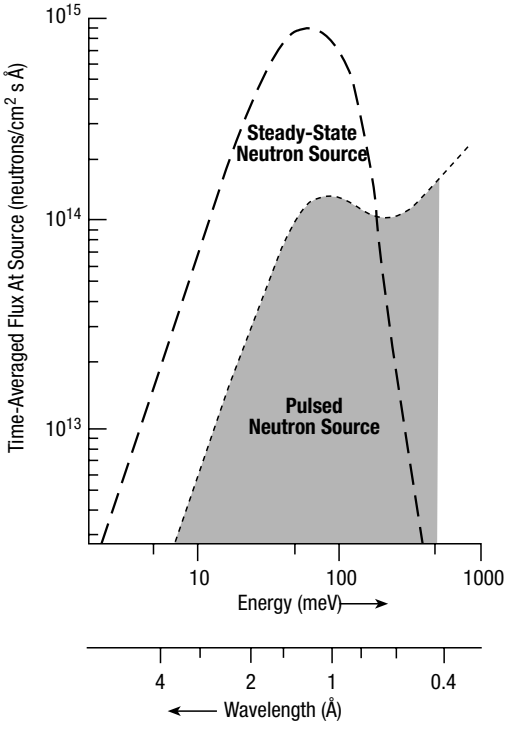

Fig. 1.3. Comparison of the source spectra of a steady-state reactor and a pulsed neutron source (from Windsor, 1981).

shown schematically in Fig. 1.3. For both types of sources the neutrons have to be moderated in order to reduce the effective neutron temperature to near room temperature. In a reactor, the flux is nearly isotropic and approximates a Maxwellian distribution of the neutron velocities with characteristic temperature of ~ 350 K. The typical useful energy range of "thermal" neutrons is 5–100 meV; "cold" neutrons from a cryogenic moderator are roughly in the range of 0.1–10 meV. There is a relatively small epithermal (> 100 meV) contribution, and this is beneficial for achieving a low background in the thermal regime. A spallation source has a much higher epithermal content in the energy spectrum, and the pulsed sources have a distinct advantage in exploiting this energy region. At a reactor, a useful flux in this higher-energy range can be provided with a "hot" source; the hot moderator at ILL consists of a block of graphite heated to 2400 K.

The pulsed beam from a spallation source is well suited to time-of-flight techniques. In one type of spectrometer, the incident neutrons are monochromatized using one or more choppers, and the energies of scattered

neutrons are determined by the time it takes them to reach the detector. With the use of large arrays of position-sensitive detectors, it is possible to measure large regions of energy transfer, $\hbar\omega$, and momemtum transfer, $\hbar\mathbf{Q}$, simultaneously. At a reactor, neutron energy selection is more commonly achieved with Bragg-diffraction optics. The ability to focus neutrons onto the sample with a curved monochromator provides advantages for studies concentrating on a small region of ω–$\mathbf{Q}$ space.

1.3 Reciprocal space and scattering diagram

The laws of momentum and energy conservation governing all diffraction and scattering experiments are well known:

$$\mathbf{Q} = \mathbf{k}_f - \mathbf{k}_i \qquad \text{(momentum conservation)} \tag{1.2}$$

$$|\mathbf{Q}| = k_i^2 + k_f^2 - 2k_i k_f \cos\theta_S \tag{1.3}$$

$$\hbar\omega = E_i - E_f \qquad \text{(energy conservation).} \tag{1.4}$$

In these equations, the wave-vector magnitude $k = 2\pi/\lambda$, where λ is the neutron wavelength of the neutron beam, and the momentum transferred to the crystal is $\hbar\mathbf{Q}$. The subscript i refers to the beam incident on the sample and f the final or diffracted beam. The angle between the incident and final beams is $2\theta_S$ and the energy transferred to the sample is $\hbar\omega$. It is important to note that our sign convention for $\mathbf{Q}$ is the same as that used by Bacon (1975) but opposite to that of Lovesey (1984), who defines $\mathbf{Q}$ as $\mathbf{k}_i - \mathbf{k}_f$. The sign choice has implications for the resolution function discussed in Chap. 4.

Because of the finite mass of the neutron the dispersion relation for the neutron is:

$$E = \frac{\hbar^2 k^2}{2m_n},$$

$$E[\text{meV}] = 2.072k^2[\text{Å}^{-2}], \tag{1.5}$$

and the energy conservation law can be written as

$$\hbar\omega = \frac{\hbar^2}{2m_n}(k_i^2 - k_f^2). \tag{1.6}$$

Energy units are usually measured in meV, or equivalently as E/h in terahertz (THz $= 10^{12}$ Hz). Table 1.5 gives the energy relationships for neutrons in various units and their values at 10 meV. In this monograph we shall use mainly meV energy units. Wavelength, λ, and wave vector, k, will be expressed in Å and Å^{-1} units, respectively, where $1\,\text{Å} = 10^{-8}\,\text{cm} = 0.1\,\text{nm}$.

Table 1.5. *Wavelength, frequency, velocity and energy relationships for neutrons.*

Quantity	Relationship	Value at $E = 10\,\text{meV}$
Energy	$[\text{meV}] = 2.072k^2[\text{Å}^{-1}]$	10 meV
Wavelength	$\lambda[\text{Å}] = 9.044/\sqrt{E[\text{meV}]}$	2.86 Å
Wave vector	$k[\text{Å}^{-1}] = 2\pi/\lambda[\text{Å}]$	2.20 Å^{-1}
Frequency	$\nu[\text{THz}] = 0.2418E[\text{meV}]$	2.418 THz
Wavenumber	$\nu[\text{cm}^{-1}] = \nu[\text{Hz}]/(2.998 \times 10^{10}\,\text{cm/s})$	$80.65\,\text{cm}^{-1}$
Velocity	$v[\text{km/s}] = 0.6302\,k[\text{Å}^{-1}]$	1.38 km/s
Temperature	$T[\text{K}] = 11.605E[\text{meV}]$	116.05 K

In any scattering experiment one always measures the properties of the incident (i) and final (f) neutron beams and infers the momentum and energy transferred to the sample via Eqs. (1.2) and (1.6). Since thermal neutrons have energies similar to those of many excitation processes of interest in solids (see Fig. 1.4), a rather modest and easily achievable energy resolution of $\Delta E/E \sim 10\%$ is frequently sufficient to obtain useful results. This is quite different from the case of inelastic scattering with X-rays or electrons, where, because of the larger probe energy ($\sim 10\,\text{keV}$ for X-rays), a comparable absolute uncertainty ΔE may require $\Delta E/E \sim 10^{-7}$.

1.3.1 Elastic scattering

For the moment, let us consider only elastic scattering in a crystalline solid, i.e., $|\mathbf{k}_i| = |\mathbf{k}_f| = k$. To understand diffraction and scattering measurements, it is necessary to deal with the reciprocal lattice of the solid. The dots in Fig. 1.5 represent a reciprocal lattice for a two-dimensional crystalline solid, with each point corresponding to a reciprocal-lattice vector. If we plot a circle with radius k on this diagram such that it passes through two points on the circle, one of which is the origin of reciprocal space, the condition for Bragg scattering from the crystal is satisfied. The circle is called the Ewald circle in two dimensions, or the Ewald sphere in three dimensions. In the diagram, $\mathbf{k}_i$ is the direction of the incident beam relative to the crystal and $\mathbf{k}_f$ is the direction of the diffracted beam. For the case satisfying the Bragg condition:

$$\mathbf{Q} = \mathbf{G} = \mathbf{k}_f - \mathbf{k}_i \tag{1.7}$$

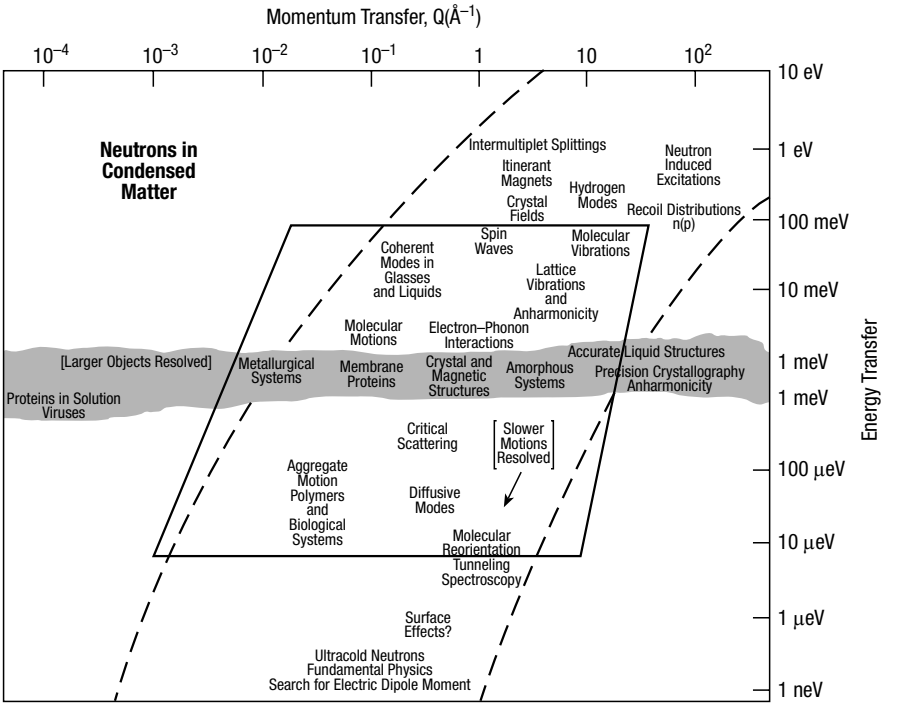

Fig. 1.4. Various applications of inelastic neutron scattering in terms of energy and momentum transfer. The region inside the trapezoidal box is the approximate range probed by three-axis instruments (from Lander and Emery, 1985). (The shaded region corresponds to an expanded cut in the energy scale.)

where $\mathbf{G}$ is a reciprocal-lattice vector. From Eq. (1.3) and Fig. 1.5

$$|\mathbf{Q}| = |\mathbf{G}| = 2|\mathbf{k}_i| \sin\theta_S, \tag{1.8}$$

where $2\theta_S$ is the angle between the incident and the final beam for the Bragg condition. This is the well-known Bragg's law, which can also be written in the more familiar form

$$\lambda = 2d \sin\theta_S \tag{1.9}$$

by noting that the magnitude of the reciprocal-lattice vector $|\mathbf{G}| = 2\pi/d$ where d is an interplanar spacing.

In a diffraction experiment, the magnitude of $\mathbf{Q}$ is controlled by adjusting the angle $2\theta_S$ between $\mathbf{k}_i$ and $\mathbf{k}_f$. The orientation of $\mathbf{Q}$ within the reciprocal lattice is set by rotating the sample. Thus, any point in reciprocal space can be measured by an appropriate choice of $\mathbf{k}_i$, $2\theta_S$, and the orientation ϕ of the sample relative to $\mathbf{k}_i$.

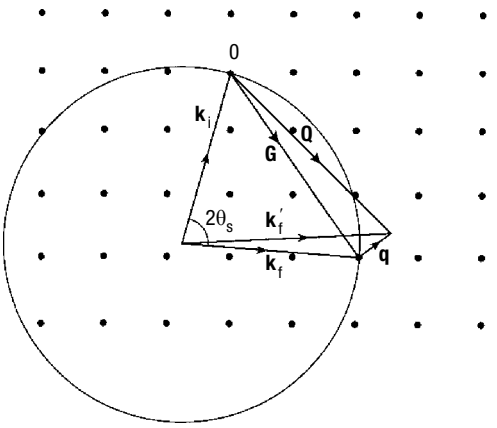

Fig. 1.5. Two-dimensional representation of reciprocal space showing the Ewald circle and the vector representation for elastic and inelastic scattering. Here **G** is a reciprocal-lattice vector and **q** the momentum transfer within the first Brillouin zone (see § 1.3.2 and Fig. 1.6).

1.3.2 Inelastic scattering

For inelastic neutron scattering, the situation is more complicated. In this case $|\mathbf{k}_i| \neq |\mathbf{k}_f|$ since a difference is needed in order to transfer energy to the sample. In an experiment, one typically holds one wave vector (k_i or k_f) constant while varying the other. For a single-crystal sample, energies depend only on the relative momentum $\hbar\mathbf{q}$ defined within a Brillouin zone; hence, it is convenient to reference the momentum transfer to the nearest reciprocal lattice vector, i.e.,

$$\mathbf{Q} = \mathbf{G} + \mathbf{q}, \tag{1.10}$$

as illustrated in Fig. 1.6. The measured spectrum can be interpreted straightforwardly if **Q** is held constant while the energy transfer is varied. Figure 1.6 shows two cases where k_i is kept constant and k_f varies. In the first situation [Fig. 1.6(a)], with $k_i > k_f$ and $\hbar\omega > 0$, energy is transferred from the incident neutron to the sample and an excitation is created; this is equivalent to Stokes scattering in optical spectroscopy. In the second example [Fig. 1.6(b)], $k_i < k_f$ and $\hbar\omega < 0$, so that the sample gives up a quantum of energy to the neutron beam. An excitation is annihilated and we have neutron energy gain (or anti-Stokes scattering).

In order to keep **Q**, and thus **q**, constant while varying $\mathbf{k}_f$, the scattering angle must change as well as the relative orientation of the crystal with respect to $\mathbf{k}_i$. The schematic in Fig. 1.6 shows the lattice staying fixed and

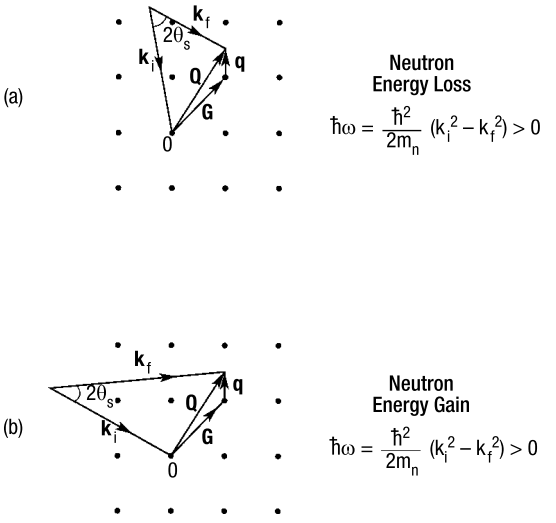

Fig. 1.6. Vector diagrams of inelastic scattering for (a) neutron energy loss ($k_f < k_i$), (b) neutron energy gain ($k_f > k_i$). 0 represents the origin of reciprocal space, **G** a reciprocal-lattice vector, and **q** the momentum transfer within a zone.

$\mathbf{k}_i$ moving. In practice, it is the other way around: $\mathbf{k}_i$ is kept fixed in space while the crystal is rotated.

1.4 Neutron scattering instruments

The main focus of this monograph is the triple-axis (or three-axis) spectrometer, which is an effective tool for both elastic and inelastic scattering studies. Here we compare it briefly with three other types of instrument commonly used for inelastic studies (see Fig. 1.7): time-of-flight (TOF), backscattering, and neutron spin-echo spectrometers.

1.4.1 Three-axis instrument

The three-axis instrument is the most versatile and useful instrument for use in inelastic scattering because it allows one to probe nearly any coordinates in energy and momentum space in a precisely controlled manner. The brilliant concept was developed over 40 years ago by Brockhouse (1961) at Chalk River in Canada. The three axes correspond to the axes of rotation of the monochromator, the sample, and the analyzer. The monochromator defines the direction and magnitude of the momentum of the incident beam and the analyzer performs a similar function for the scattered or final beam.

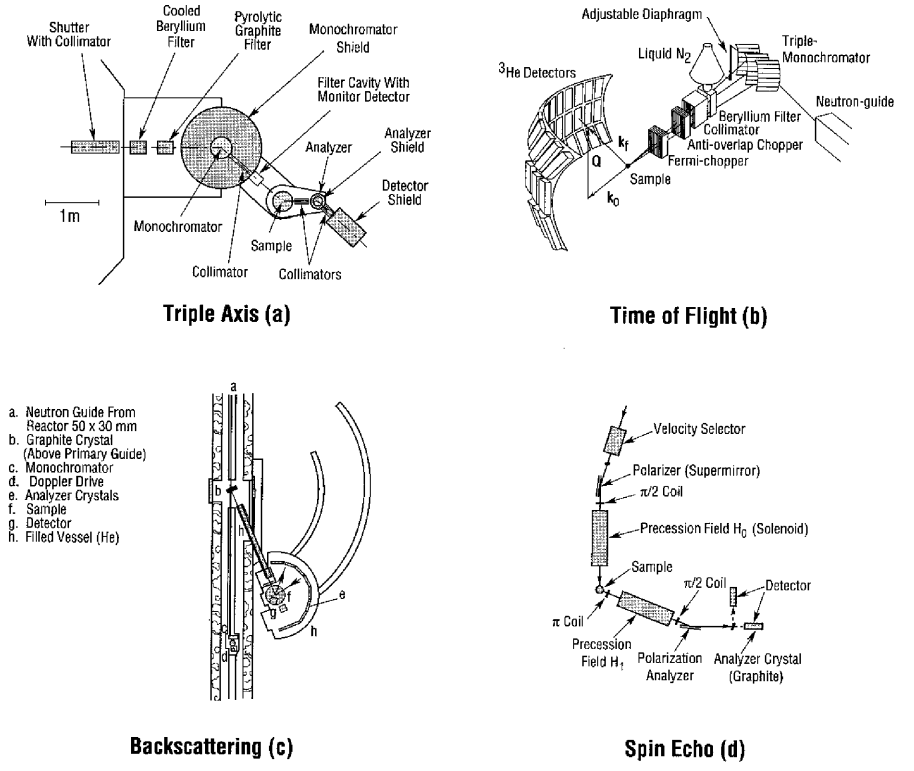

Fig. 1.7. Several types of spectrometers used at steady-state sources.

Figure 1.2(b) shows the three-axis instruments formerly situated at the H7 and H8 beam ports at BNL. Inside the large semi-cylindrical structure is the monochromator, and neutrons diffracted by it hit the sample. Those neutrons scattered by the sample are Bragg reflected by the analyzer, which lies within the white shielding. The instrument is large, mainly because of the necessary shielding which keeps the radiation levels low in the neighborhood of the instrument and keeps the background measured by the detector at the lowest possible level. The various components of the three-axis spectrometer, shown in Fig. 1.7(*a*), will be discussed in Chap. 3.

1.4.2 Time-of-flight (TOF) instrument

The time-of-flight technique was first employed to perform energy-dependent neutron measurements (Dunning *et al.*, 1935). The technique has been greatly refined over the last 50 years with the advent of reactors and pulsed sources, but the principles remain the same. In the TOF technique, a burst of

polychromatic neutrons is produced, and the times taken by the neutrons to travel from the source of the burst to the detector (counter) are measured. After interacting with the sample, the neutron will gain or lose energy, resulting in a velocity change. The arrival time at the counter will therefore vary.

If the neutron source is a reactor, a chopper or combination of choppers is used to define the initial pulse at time t_0. Frequently, instead of a chopper, a rotating crystal is used which simultaneously monochromatizes and pulses the neutron beam before it is scattered by the sample. Pulsed sources, by their nature, are ideally suited for TOF techniques. The pulse of polychromatic neutrons is provided by the accelerator, and the chopper, which is usually synchronized with the accelerator, defines the time t_0.

Figure 1.7(b) shows a schematic of the IN5 TOF spectrometer at ILL in Grenoble. This instrument is designed to give high energy resolution ($\sim 3\mu$eV) and is situated at a cold source. Two synchronized choppers are used to define the incident beam energy, while a third chopper is used to eliminate unwanted neutrons with velocities that are integral multiples of the desired neutron velocity. The fourth chopper spins at a lower speed in order to prevent frame overlap from different pulses. In this spectrometer the sample is placed in an argon-filled sample box allowing for a wide range of sample environments. The scattered neutrons then travel over a distance of about 4 meters to a number of detectors covering the angular range $-10^\circ \leq 2\theta_S \leq 130^\circ$. This instrument has a wide range of inelastic neutron scattering applications; notable among them are studies of tunneling states in hydrogen-containing materials.

1.4.3 Backscattering and neutron spin echo (NSE)

Figures 1.7(c) and 1.7(d) show two instruments used to achieve very high energy resolution. The backscattering instrument (Birr, Heidemann, and Alefield 1971; Alefeld, Springer, and Heidemann, 1992) uses very good crystals with narrow mosaics for monochromator and analyzer, each with a fixed Bragg angle of $\sim 90^\circ$. Since one cannot scan in energy by varying the angle of the monochromator, the incident energy is instead tuned by a Doppler drive attached to the monochromator. Another method for scanning energy is to vary the temperature of the crystal, so that the lattice spacing of the monochromator is changed while keeping the scattering angle fixed. The new High Flux Backscattering Spectrometer at NCNR has achieved an energy resolution of $< 1\,\mu$eV with a dynamic range greater than $\pm 40\,\mu$eV (Gehring and Neumann, 1998).

The neutron spin echo (NSE) technique is a novel one developed (Mezei, 1972) to obtain high energy resolution without the concommitant intensity losses associated with backscattering geometries and the use of nearly perfect crystals. It relies on the use of polarized beams traversing a magnetic field region and the measurement of the number of precessions the neutron makes before and after hitting the sample. The schematic of an NSE spectrometer, the IN11 at ILL, is shown in Fig. 1.7(d). A cold source emits a neutron beam with a relatively broad band of energies which is then polarized by a supermirror. The spin of the neutron is flipped so that it is perpendicular to the magnetic field of the solenoid. The neutron will then make a number of Larmor precessions which depend upon the field strength and the length of the field region. The neutrons then strike the sample and gain or lose a small amount of energy. The spins are flipped 180° and enter a second precession field where they precess in the opposite direction. The spins are then flipped by 90° so they can be analyzed and detected. The difference between the number of precessions before and after the sample is proportional to the change in the velocity of the neutron after interacting with the sample. In this technique, since the precession of each neutron is measured, the resolution of the neutron energy transfer is independent of the beam monochromatization. The quantity measured is not the usual scattering function, $S(\mathbf{Q},\omega)$, but its time-dependent Fourier transform, $S(\mathbf{Q},t)$. If one compares the effective energy resolution by converting from the time domain, the NSE is able to achieve neV resolution, much better than that obtainable with more conventional instruments. This instrument is especially useful in probing the dynamics of macromolecular systems where large molecules move very slowly. It complements optical correlation spectroscopy by being able to probe a much larger range of momentum transfer.

References

Alefeld, B., Springer, T., and Heidemann, A. (1992). *Nucl. Sci. Eng.* **110**, 84.
Bacon, G. E. (1975). *Neutron Diffraction* (Clarendon Press, Oxford).
Bacon, G. E. (1986). *Fifty Years of Neutron Diffraction: The Advent of Neutron Scattering*, ed. G. E. Bacon (Adam Hilger, Bristol).
Birr, M., Heidemann, A., and Alefeld, B. (1971). *Nucl. Instrum. Methods* **95**, 435.
Brockhouse, B. N. (1961). In *Inelastic Neutron Scattering in Solids and Liquids* (International Atomic Energy Agency), p. 113.
Dunning, J. R., Pegram, G. B., Fink, G. A., Mitchell, D. P., and Segre, E. (1935) *Phys. Rev.* **49**, 704.
Gehring, P. M. and Neumann, D. A. (1998). *Physica B* **241–243**, 64.
Lander, G. H. and Emery, V. J. (1985). *Nucl. Instrum. Methods B* **12**, 525.

Lovesey, S. W. (1984). *Theory of Neutron Scattering from Condensed Matter* (Clarendon Press, Oxford).
Mezei, F. (1972). *Z. Phys.* **255**, 146.
Price, D. L. and Sköld, D. L. (1986). In *Methods of Experimental Physics, Vol. 23: Neutron Scattering*, ed. K. Sköld and D. L. Price (Academic Press, Orlando), Part A, p. 1.
Windsor, C. G. (1981). *Pulsed Neutron Diffraction* (Taylor Francis, London).